# Resolved imaging of extra-solar planets with future 10−100 km optical interferometric arrays

A. Labeyrie

Collège de France & Observatoire de Haute Provence (CNRS), F-04870 Saint Michel l'Observatoire, France
E-mail labeyrie@obshpx.obs-hp.fr

**Abstract.** — In the recent years, interferometric arrays of optical telescopes have reached sizes of the order of 100 m, but they have yet to produce high-resolution images. The analysis of image formation now shows that such images are theoretically obtainable directly in the recombined focal plane, if there are enough telescopes. Resolved images of extra-solar planets are in principle obtainable with 10 km ground-based arrays.

**Key words:** techniques: interferometric planetary systems

## 1. Introduction

The recent spectroscopic detection of periodic velocity changes on the star 51 Peg provides likely evidence for the presence of a planet (Mayor & Queloz 1995). Images showing such extra-solar planets as unresolved dots near their parent stars will perhaps be obtained within a decade, using coronographic telescopes in space or on Earth (Bonneau et al. 1975; Ken Knight 1977; Bracewell 1979; Burke 1986; Brown 1990; Angel 1994; Labeyrie 1995; Malbet et al. 1994). A subsequent step will be the formation of resolved images showing some detail of these planets. At optical wavelengths, this will require apertures in the size range from 1 to 100 km, to be achieved in the form of multi-element interferometric arrays.

Ever since light from separate telescopes could be recombined and made to interfere (Labeyrie 1975), larger systems became used and provided high-resolution data (Mourard et al. 1994; Mariotti 1992), although not in the form of images. Interferometrically coupled telescopes became then considered for the major new projects in optical astronomy, such as ESO's four 8 m telescopes and the pair of 10 m Keck telescopes. For "snapshot" imaging, i.e. the formation of a usable high-resolution image in a single exposure lasting minutes, plans are also made for a dedicated interferometric system of many 1.5 m telescopes, the Optical Very Large Array or OVLA (Labeyrie et al.1992). The initial design involves a 600 m ring with 27 telescopes, but later expansion to sizes beyond one or ten kilometers is considered. The corresponding angular resolution will increase from $10^{-4}$ to $10^{-5}$ arcsec. In space, 100 km arrays with superior sensitivity and $10^{-6}$ arcsec resolution are probably feasible.

This article outlines a theory of image formation in multi-element optical arrays. It shows that resolved images of extra-solar planets are in principle obtainable from the ground, as well as in space.

## 2. Imaging properties of diluted optical arrays

Fizeau's 1868 proposal to install a mask with two holes, or sub-apertures, on top of a telescope allowed Michelson to resolve the satellites of Jupiter. For improved resolution, he subsequently increased the baseline span beyond the size of the largest telescope then available by installing on top of it, "in periscopic fashion", a 20 feet (6.5 m) beam carrying four flat mirrors. Such optical configurations can be extrapolated towards large arrays of many elements, all of which may be considered as sub-apertures of a single giant optical aperture.

The sub-apertures used by Michelson were not much larger than the size of atmospheric turbulence cells. The following discussion assumes sub-apertures of arbitrary size, but equipped with adaptive optics to provide diffraction-limited "sub-images" (i.e. images formed by each sub-aperture), all of which are recombined in a single image where interference occurs (see Fig. 1). For fully constructive interference, in the presence of instrumental and atmospheric phase shifts, each sub-image is also adaptively phased, for example by translating a mirror with a fast actuator.
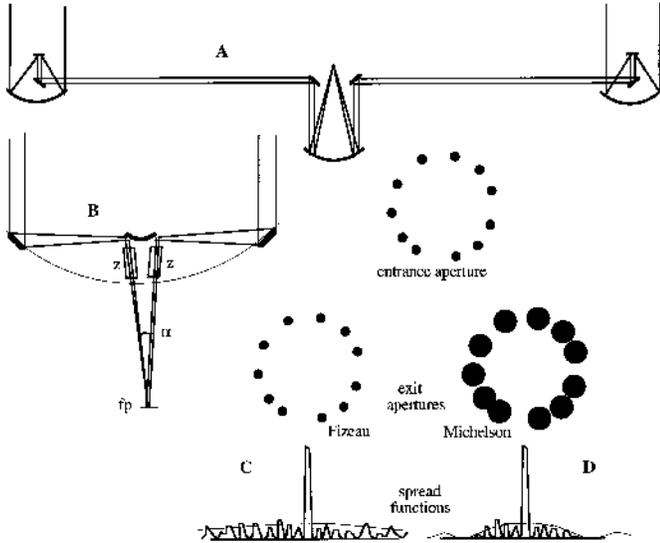
**Fig. 1.** Principle of Fizeau and Michelson configurations for a large multi-element interferometer (A,B). A is equivalent to Michelson's periscopic train, while zoom lenses Z on each beam of the telescope-like array B provide adjustable conversion from Fizeau to Michelson geometries. The zoom lenses are assumed to preserve the image focus while changing the image scale. They can be adjusted from a neutral position, providing the 1x image magnification corresponding to the Fizeau geometry (C), towards increasingly demagnified images providing Michelson's wider sub-pupils (D). The variable focal ratio in the sub-images leaves the array's global focal ratio $1/\alpha$ nearly invariant, thus not affecting the scale of the fine interference structure. When zooming however, the image's Airy envelope varies in size since it is the diffraction pattern of the sub-apertures

When utilized to construct such multi-aperture arrays, the "periscopic" principle of Michelson provides a somewhat un-natural imaging configuration since the multi-element exit pupil is re-arranged with respect to the entrance pupil, the relative size of the sub-pupils being increased at the exit (see Fig. 1). One can also arrange to have the sub-pupil centers displaced with respect to their arrangement in the entrance pupil, however such arrays do not have the field-invariant interference function considered in this article. The following discussion is restricted to the class of Michelson arrays, hereafter called "conformal", where the pattern of sub-pupil centers is identical in the entrance and exit pupils.

With the increased relative size of the sub-pupils, the sub-images are shrunk with respect to the interference patterns which they form when becoming superposed at the common focus. When the source moves off-axis, the fringes move faster than the sub-images. Tallon & Tallon-Bosc (1992) have shown that the ensuing image degradation can be corrected post-detection. I show now that conformal Michelson arrays can provide directly usable high-

resolution images at their focus, with a significant gain in signal/noise ratio.

Figure 1 sketches two equivalent configurations for a large multi-element Michelson interferometer. Each is adjustable, in terms of the "pupil concentration coefficient". $\gamma_d = [d_o/D_o]/[d_i/D_i]$ where $D_i$ and $d_i$ are the entrance pupil diameters, respectively for the array and the sub-apertures, while $D_o$ and $d_o$ are the corresponding diameters in the exit pupil. In the Fizeau mode $\gamma_d = 1$. For an "extreme Michelson array" having its exit pupil completely filled according to a square or hexagonal grid pattern of sub-pupils, $\gamma_d = N^{-1/2} D_i d_i^{-1}$. With a 10 km array of 100 elements, each 1.5 m in size, arranged on a square grid so as to provide a $10 \times 10$ filled array in the exit pupil, $\gamma_d = 666$. A comparable value is obtained with a ring-shaped array of 27 elements, other things equal.

According to classical diffractive optics, the monochromatic image of a point source is the Fourier transform of the distribution of complex amplitudes in the pupil. When dealing with a Michelson array, the pupil to be considered is the exit pupil since the wavefront has no memory of its arrangement in the entrance pupil. Given the adaptive optics which smoothes the phase in each of the sub-apertures, the pupil function may be considered as a convolution of a uniform disc representing the sub-aperture function, with an array of Dirac peaks representing the array function. The focal pattern is then a product of the broad Airy pattern diffracted by the sub-apertures with the finer interference pattern diffracted by the array of Dirac peaks. Their respective scale varies in proportion to $\gamma_d$.
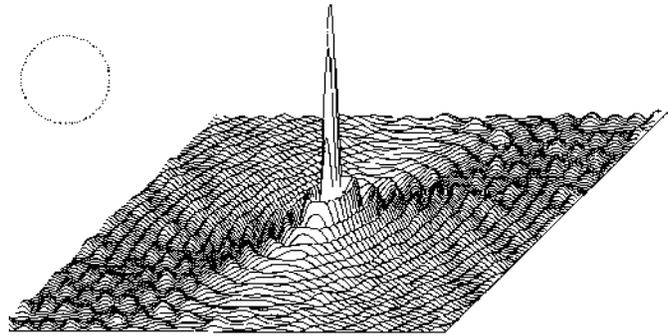


**Fig. 2.** Example of interference function, obtained as the Fourier transform of 100 Dirac peaks, randomly arrayed along a circle (top) and cophased. The central part resembles an Airy disk, with concentric rings, but, towards the periphery, these are increasingly broken into random speckles

With many phased sub-apertures, the interference pattern is dominated by a central peak (see Fig. 2), the intensity of which is $N$ times the locally averaged intensity of the surrounding halo of side-lobes. This halo being multiplied by the Airy function, which may be considered as a window limiting the pattern size, the $\gamma_d$ settings affect

the fraction $q_e$ of energy contained in the peak, according to the expression:

$$q_e = N \left(\frac{d_o}{D_o}\right)^2 = N \left(\frac{\gamma_d \, d_i}{D_i}\right)^2 \quad (1)$$

The fraction is very small for highly diluted Fizeau arrays, but approaches $\pi^2/N$ for a ring geometry at maximal zoom settings, i.e. when the sub-pupils fill the perimeter of the exit pupil (because $N$ is assumed larger than 10, there is no risk that $q_e$ might exceed 1). $q_e = 1$ for extreme Michelson arrays.

In the exit pupil, the wavefront provided by a phased array is discontinuous but flat (one considers for simplicity that the exit pupil is very small with respect to its distance to the recombined image plane). If the source now moves away, the wavefront propagating through the exit pupil acquires a stair-shaped profile (see Fig. 3). The wavefront elements in each sub-pupil indeed remain parallel to each other, but the average exit wavefront is tilted since the Michelson arrangement amplifies the optical delays in its arms. However, the facet centers define an average wavefront which is still a plane if the patterns of the centers are identical in the entrance and exit pupils, as is the case for the conformal Michelson arrays considered here (field aberrations can distort this plane, particularly if the periscopic optics has mirrors which are not plane, but this is a higher-order effect, to be discussed elsewhere).

Therefore, fully constructive interference can still occur, but in the direction orthogonal to the average stair plane rather than to the facets. This direction is tilted by an angle $\gamma_d \, \alpha$ when the source has moved through an angle $\alpha$ on the celestial sphere, while the facet's normal is also tilted by $\alpha$. With respect to the sub-aperture's Airy profile, the complete interference function $I(x,y)$ is thus translated together with its peak, and therefore becomes excentered (see Fig. 1D) but otherwise unchanged. Its product with the Airy function $A(x,y)$ still defines the resulting diffraction pattern in the recombined focal plane, since the wavefront in the exit pupil may again be considered as a convolution of disks with a tilted plane array of Dirac points.

The distribution of intensities in the recombined image of a monochromatic point source may thus be expressed as:

$$B_p \,(x,y,\alpha,\beta) = I(x+\gamma_d \, \alpha, y+\gamma_d \, \beta) \, A(x+\alpha, y+\beta) \quad (2)$$

where $\alpha, \beta$ are the field angles defining the source's position with respect to the axis .

Changing the wavelength does not affect the position of the peak, only its width, nor the position of the Airy envelope, but only its width. This description has some
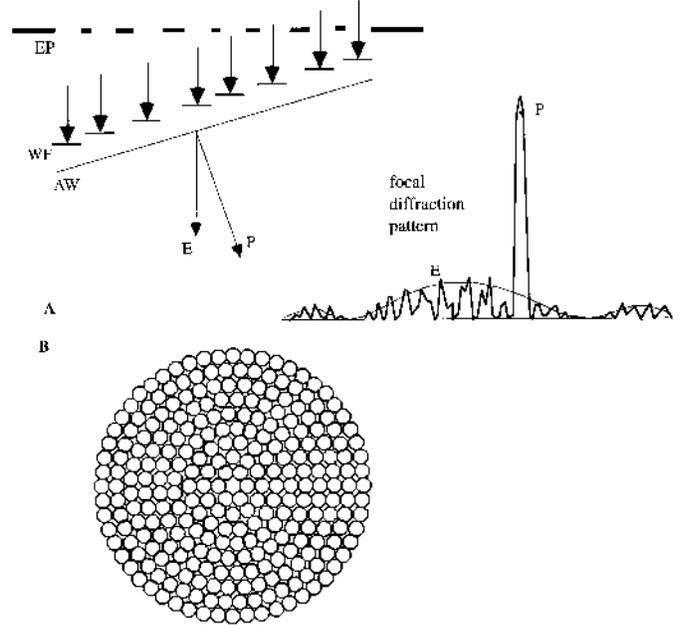


**Fig. 3.** A- Field invariance of the interference function in a conformal Michelson array. If a point source moves away from the field position where phasing is achieved, the wavefront WF at the exit pupil EP is no longer flat but stair-shaped. Its average slope, with respect to the steps, is proportional to the source's displacement. Considered as a convolution of tilted discs with a plane array of points, located in the average wavefront AW, WF provides a focal diffraction pattern which is a product of a broad Airy envelope E with a decentered interference function P, having a peak with side-lobes. Their directions are respectively orthogonal to the steps and to AW. Both functions are field-invariant, but with a different motion velocity in response to the source's motion: owing to the baseline leverage effect, the peak moves faster than the Airy envelope when a star crosses the field. A star or planet, being typically resolved by the peak and not by the envelope, thus provides a resolved image appearing on the envelope background. B- Example of a nearly-filled exit pupil with 278 elements, according to the "extreme Michelson mode". It can be obtained for example with 1.5 m telescopes spaced 526 m apart, along 9 concentric circles, thus forming a 10 km array. In its central region, the interference function differs little from an Airy pattern. The diffraction envelope, also an Airy pattern, is 18 times wider, thus providing on an extended object a direct image with 18×18 resolved elements

analogy with the classical theory of blaze effects in diffraction gratings having stair-shaped grooves. Since the interference function $I(x,y)$ is itself field-invariant, the aberrations being neglected, an extended incoherent object causes a convolution of its intensity, thus generating an image if $I(x,y)$ is prominently peaked. But the nearly stationary Airy window $A(x,y)$ introduces complications with respect to the classical convolution description of image formation, applicable to a Fizeau array: there is no longer a stable spread function to be convolved with the

object. It obviously limits the imaging field available in a snapshot exposure; and the classical convolution becomes a pseudo-convolution of the form:

$$B(x,y) = \int \int O(\alpha, \beta) \; I(x \; + \; \gamma_d \; \alpha, y \; + \gamma_d \; \beta)$$

$$. \; A(x + \alpha, y + \beta) \; d\alpha \; d\beta \qquad (3)$$

where $O(\alpha, \beta)$ describes the intensity distribution in the observed object and $B(x,y)$ describes the intensity distribution in the image.

A more convenient, but approximate, expression may be derived for use in the practical cases considered here, where the approximation introduces negligible errors. Since the array is highly diluted and the object very small, $\gamma_d \gg 1$ and $\alpha, \beta \ll 1$ , then the dependance of $A(x + \alpha, y + \beta)$ with respect to the field position $\alpha, \beta$ becomes negligible and Eq. (3) may be written:

$$B(x,y) \approx A(x,y) \int \int O(\alpha, \beta) \; I(x + \gamma_d \alpha, y + \gamma_d \beta) \; d\alpha \; d\beta$$

$$B(x,y) \approx \gamma_d^{-2} \; A(x,y) \int \int O(\alpha, \beta)$$

$$. \; I(x + \gamma_d \; \alpha, y \; + \; \gamma_d \; \beta) \; d\gamma_d \; \alpha \; d\gamma_d \; \beta$$

$$B(x,y) \approx \gamma_d^{-2} \; A(x,y) \left[ O\left( \frac{x}{\gamma_d} \; , \; \frac{y}{\gamma_d} \right) \; \otimes \; I(x,y) \right] \qquad (4)$$

where $\otimes$ indicates a convolution. It shows that the image is formed by an ordinary convolution, followed by a multiplication having the effect of a window.

When the array is phased within the Rayleigh tolerance, the resulting peak in the interference function becomes convolved with the object inside the Airy window, the size of which is adjustable by changing $\gamma_d$. It provides a directly usable image if one removes the pedestal caused by the convolution of the side-lobes. This is achievable by subtracting the average pedestal level, or preferably by deconvolving with the known interference function $I(x,y)$. In the case of an extreme Michelson array (see Fig. 3B), the filled exit pupil provides an interference function $I(x,y)$ which is similar in its central part to the diffraction pattern of the corresponding filled aperture.

## 3. The signal to noise ratio

Images of a small object are directly generated in a usable form, with a single exposure, if the number of baselines exceeds the number of resolved object points, and if there is adequate signal /noise ratio. In the case of a faint and small object such as an extra-solar planet, the signal/noise ratio is dominated by photon noise rather than by the side-lobe convolution. The number of resolved elements within a planet's apparent disc of angular size $s_p$ is:

$$n_p = \left( s_p \frac{D_i}{\lambda} \right)^2 \qquad (5)$$

With respect to the planet's photon count $F_p$ entering the array aperture, of which a fraction $q_e$ contributes to the formation of the resolved planet image, each resolved element receives a fraction $1/n_p$. In the convolved peak, the photon count from the planet per resolved element is therefore

$$f = F_p N \left( \gamma_d \quad d_i \; \frac{\lambda}{s_p} \right)^2 D_i^{-4}$$

where the optimal value $\gamma_{opt}$ of the pupil concentration coefficient may somewhat arbitrarily be considered to be such that the resolved planet fits within the Airy profile:

$$s_p \frac{D_i}{\lambda} = \frac{D_o}{d_o} = \frac{D_i}{\gamma_{opt} d_i} \; , \quad \text{giving} \quad \gamma_{opt} = \frac{\lambda}{s_p d_i}$$

therefore

$$f \; = \; F_p \; N \; \lambda^4 \; s_p^{-4} \; D_i^{-4} \qquad (6)$$

for the Michelson mode with a pupil concentration coefficient adapted to the planet size, whereas the Fizeau mode gives a photon count $f = F_p N \left( d_i \frac{\lambda}{s_p} \right)^2 D_i^{-4}$ which is much lower.

The photon count per elementary area of the pedestal, i.e. an area equal to the unconvolved peak's area, is:

$$f_h = f \; n_p \; N^{-1} = F_p \; n_p \; \lambda^4 \; s_p^{-4} \; D_i^{-4} \qquad (7)$$

since each resolved planet element has a peak $N$ times brighter than its averaged side-lobe intensity.

An extra-solar planet being very close to its parent star, one must also add to the pedestal level the star's contribution, from its speckled halo of diffracted light.

At the scale of the Airy envelope it amounts to $F_s/(G g_{ds})$ where $F_s$ is the total stellar photon count obtainable from the $N$ telescopes; $G = \sigma^{-2}(d_i/\Delta x)^2$ is Angel's "adaptive gain" (Angel 1994), here describing the peak/halo intensitiy ratio for a single sub-aperture, and $g_{ds}$ is the additional gain achievable by instructing the adaptive system at each telescope to darken the particular sub-image speckle located at the planet's position. $\sigma$ is the residual RMS phase error within a sub-pupil, and $\Delta x$ is the size of the actuators. Such adaptive darkening is most efficient in space (Malbet et al. 1994; Labeyrie 1995) but, on the ground, it can still decrease by an order of magnitude the local starlight level. The local darkening of starlight at the planet's position in each sub- image obviously benefits the recombined image, in terms of starlight contamination within the faint planet image. Although the passive exploitation of dark speckles, randomly occurring in response to residual wave bumpiness, appears preferable

for searching exo-planets with an adaptive telescope, the adaptive form of speckle darkening becomes more efficient once the position of a planet is known.

At the smaller scale of the fine resolution element, the star's contribution to the planet image is $[F_s/(G\ g_{ds})]\ (d_o/D_o)^2$, or $[Fs/(G\ g_{ds})]\ (D_i\ s_p/\lambda)^{-2}$ if the pupil concentration coefficient is optimized, as defined above, to fit the planet image in the Airy profile.

Thus, the total count in the pedestal of the planet image, per elementary area, is:

$$
\begin{aligned}
f_b \ =\ & F_p\ n_p\ \lambda^4\ s_p^{-4}\ D_i^{-4} \\
& +\ F_s\ \sigma^2 \left(\frac{d_i}{\Delta x}\right)^{-2}\ g_{ds}^{-1}\ (D_i\ s_p)^{-2}\ \lambda^2
\end{aligned}
\tag{8}
$$

Its fluctuation owing to photon noise $\sqrt{f}_b$ is the dominant term defining the signal to noise ratio $S/N$ in the planet image, given the smoothing of the side-lobes achieved by the convolution and by the wavelength range used. Using the signal value given by Eq. (6), the signal to noise ratio is therefore

$$
\begin{aligned}
S/N &= \frac{f}{\sqrt{f}_b} \\
&= \frac{F_p N \lambda^4 s_p^{-4} D_i^{-4}}{\sqrt{F_p n_p \lambda^4 s_p^{-4} D_i^{-4} + F_s \sigma^2 \left(\frac{d_i}{\Delta x}\right)^{-2} g_{ds}^{-1} (D_i s_p)^{-2} \lambda^2}}
\end{aligned}
\tag{9}
$$

for the Michelson mode where the exit pupil is adjusted to image the full planet.

A better sensitivity is achievable with a filled exit pupil, according to the extreme Michelson arrangement. In this case, Eq. (6) is replaced by $f = F_p\ \lambda^2\ (s_p D_i)^{-2}$ and the pedestal becomes negligible. The star's straylight contribution per resolution element becomes $[F_s/(NG g_{ds})]$ and the signal /noise ratio

$$
\begin{aligned}
S/N &= \frac{f}{\sqrt{f}_b} \\
&= N^{1/2}\ F_p F_s^{-1/2} \lambda^2 s_p^{-2} D_i^{-2} \sigma^{-1} \left(\frac{d_i}{\Delta x}\right) g_{ds}^{1/2}
\end{aligned}
\tag{9bis}
$$

For diluted arrays pointed towards extra-solar planets, the Michelson mode thus benefits from the much higher proportion of energy in the interference peak, compared to the Fizeau mode. In the latter case, the photons are spread out in a multitude of side-lobes, the contrast of which is degraded by the convolution with the planet's disc, by chromatic effects and by the starlight contamination. Their deconvolution is heavily affected by photon noise. With a single ring of telescopes, the Michelson

mode can be optimized to match the window with the image size. With several rings, a nearly extreme Michelson arrangement can provide a nearly filled exit pupil with more severe windowing, but improved signal to noise ratio, other things equal. It also makes the exit pupil more redundant, thereby facilitating the phasing. Whether optimized to image the full object or to fill the exit pupil, the Michelson mode provides a much better signal/noise ratio than the Fizeau mode.

As an example, one may consider an array of 1.5 m telescopes, 300 of them located along a 10 km-diameter ring. A Jupiter-like planet orbiting a 1st-magnitude Sun-like star at 5 pc has an apparent magnitude $m_v = 23.5$ and is resolvable in $20 \times 20$ elements at $\lambda = 500$ nm. With the optimal Michelson recombination, each resolved element of the planet provides about 7400 detected photon events in 1000 s in the interference peak, assuming 0.6 overall quantum efficiency and a 300 nm spectral bandwidth. After pedestal subtraction, the signal-to-noise ratio in the planet image is 7.4 in 1000 s, if each telescope has 900 actuators giving 0.03 radian RMS phase residuals. With such adaptive optics, the local halo level in a sub-image is $10^6$ times fainter than in its peak, and it is assumed further darkened by a factor $g_{ds} = 10$ through speckle-darkening techniques.

A comparable signal/noise ratio is achievable with 80 telescopes of 4 m or 30 telescopes of 8 m. 1000 s is the exposure time $\tau = \pi^{-1}\ P\ n_p^{-1/2}$, where $P$ is the planet's rotation period, required to match the $20 \times 20$ element resolution with the rotational blurring of a Jupiter-like planet. At least 200 telescopes are needed if one expects to produce a usable image of the star's $200 \times 200$ resolved elements during the same exposure. If the star is not to be imaged, but serves only to activate the blind adaptive phasing in the planet, 20 apertures may suffice with some of the phasing algorithms.

With the nearly extreme Michelson arrangement shown in Fig. 3B, combining 278 telescopes of 1.5 m in a 10 km, 9-ring, array, the signal/noise ratio reaches 8.6, other things equal, but at the expanse of a slightly reduced coverage of the planetary disc, now amounting to $17 \times 17$ elements.

An Earth-like planet at 5 parsecs would require a 100 km array for resolution in $16 \times 16$ elements. If such baselines prove feasible on Earth, which appears difficult at optical wavelengths, 100 telescopes of 8 m would achieve $S/N=7.6$ in one hour, with 25.600 actuators per sub-aperture, other things equal to the previous values.

In space, the darkening of sub-image speckles at the planet's position can be more effective since there is more time to measure the residual luminosity, minutes rather than the milliseconds imposed by the atmospheric lifetime. The performance of techniques such as the "light-nulling interferometer" (Bracewell 1979) and the active formation

of dark speckles considered here should be compared in more detail. Other things equal, a 100 km space array of 36 telescopes, 4 m in size, provides $S/N = 4.8$ in the image of an Earth-like planet, with exposure time $\tau = 0.5$ hour adapted to a 24 hour rotation period. This assumes $7\ 10^6$ for Angel's gain, achieved with 5 cm actuators leaving 0.03 radian RMS phase residuals, and an additionnal 100x gain through speckle darkening. Such performance appears attainable with a group of free-flying telescopes (Labeyrie et al. 1983), as discussed below.

## 4. Phasing techniques for a star and its planet

Phasing techniques suitable for systems such as the Optical Very Large Array were previously considered (Labeyrie et al. 1986; Labeyrie et al. 1992). When attempting to produce a resolved image of an extra-solar planet, whether on Earth or in space, the parent star is a natural candidate as a reference star for adaptive phasing. Its large size, compared to the planet, however makes it highly resolved and leaves little contrast in the interference fringes. With a non-redundant exit pupil, the recombined image of a star may be Fourier transformed in real time to measure the atmospheric phases. The approximate form Eq. (4) of the pseudo-convolution Eq. (3) gives an expression for the result:

$$\tilde{B}(u,v) \approx \tilde{A}(u,v) \otimes \left[ \tilde{O}(\gamma_{\mathrm{d}}\,u, \gamma_{\mathrm{d}}\,v)\ \tilde{I}(u,v) \right] \qquad (10)$$

where wiggles indicate Fourier transforms and $u$, $v$ are coordinates in the exit pupil. Unlike the case of ordinary imaging systems, including Fizeau interferometers, one has a product of the Fourier transform of the object, classically called its visibility function, with the Fourier transform of the interference function, and the product is here convolved with the Airy function's Fourier transform. Because the Fourier transform is applied to intensities rather than complex amplitudes, the latter function is the autocorrelation function of a sub-pupil's amplitude distribution in the exit pupil. The last factor in the bracket is the autocorrelation function of the points array formed with the sub-pupil centers.

If the exit pupil is highly diluted, the result may be visualized as an array of nearly conical peaks (see Fig. 4), quasi-multiplied by the visibility function of the object. The latter generally consists of a peak surrounded by a speckled halo, since a discoïdal object may usually be modelled as a uniform disc, plus fainter detail. In the Fourier space, the model gives an Airy peak, plus a fainter speckle field.

Each of the cones in the image's Fourier transform corresponds to a pair of sub-apertures and provides phase information on the object, as well as on the atmosphere-instrument combination. Exploiting all the visibility information requires at least one cone per speckle of the

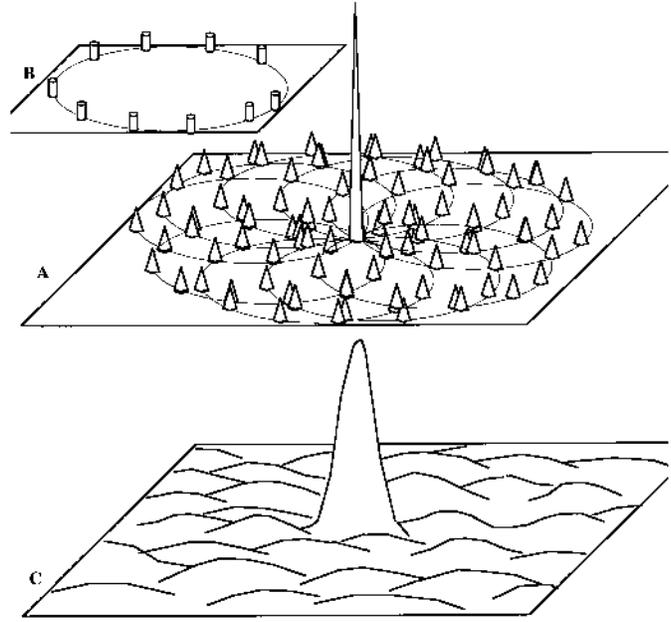visibility function, within the spatial frequency domain sampled.



**Fig. 4.** Phase closure technique for phasing low-redundancy interferometric arrays on a reference star. For a point source, the Fourier transform (A) of the recombined image is the autocorrelation of the exit pupil (B). For a resolved star, the pattern (A) is approximately multiplied by the star's complex visibility (C). To activate the adaptive corrector, the $N$ atmospheric-instrumental phases are derived from the calculated phases in the $N(N-1)/2$ cones. The inversion requires that the $N(N-1)/2$ object phases be oversampled. The object phase being smooth at the scale of the speckles in (C), some of the speckles must contain several cones. The condition may be satisfied with $N$ cones in the central peak, as achieved if the object is unresolved by the smallest baseline

Whether or not its visibility function is sampled densely enough for providing a usable image, the star can serve to activate the adaptive compensation of atmospheric plus instrumental phases needed to obtain a planet image . We can again assume that the exit pupil is non redundant ($\gamma_{\mathrm{d}}$ can be different for the star and planet, as shown in (Fig. 5) and apply the phase-closure method successfully used in the context of radioastronomical arrays: in each stellar cone, the phase given by the Fourier transformation is: $F_{ij} = F_{ij}^* + F_i + F_j$, where $i$ and $j$ are the subapertures providing the corresponding baseline, $F_{ij}^*$ is the object's phase, $F_i$ and $F_j$ are the atmospheric plus instrumental phases attached to the subapertures $i$ and $j$. The $N(N-1)/2$ baselines provide an identical number of such equations, but the number of unknowns, $N(N-1)/2 + N$, is larger. Solving for the unknown phases of the object and the atmosphere therefore requires additional information, usually provided by

redundant antennas in radio- astronomical practice. Here we can locate some of the sub-apertures for near-redundancy, for example by having a few pairs of cones closely spaced with respect to the size of the star's visibility speckles, which varies inversely with the star's size. Such pairs sample identical stellar phases, hence the redundancy.

Once the atmospheric plus instrumental phases are determined, adaptive corrections are applied to fast actuators, such as piezo-electric or electrostrictive elements, carrying one of the mirrors in each of the $N$ optical trains (see Fig. 5). Successful phasing being thus achieved for the star, it would also *ipso facto* be achieved for the planet's interference function if the atmosphere and the instrument were isoplanatic at the scale of $\lambda/4$. The atmosphere generally meets the condition for planets located within an arc-second from their parent star. The instrument, however, may have an appreciable departure from isoplanatism. In Michelson arrangements, the stair-shaped wavefront effect (see Fig. 3) may be considered as a first-order departure from isoplanatism. Higher-order terms also arise owing to aberrations. All these terms can be calculated a priori, as a function of the star-planet spacing, and can therefore be corrected in blind fashion with the small differential delay lines shown in Fig. 5 to obtain a diffraction-limited planet image centered in its Airy window.

The required low redundancy in this method favors a higly diluted exit pupil, which however affects the energy concentration. Fortunately, the $\gamma_d$ setting for the planet does not have to be the same as for the star (see Fig. 5), hence the possibility of having a little-redundant exit pupil for the star at the same time as a nearly filled exit pupil for the planet. A second difficulty results from the faint fringe visibility in the speckled feet of the star's visibility function. Whether or not there is enough signal in practice remains to be investigated. The difficulty is avoided if one has $N$ cones well within the central visibility peak or speckle, where the visibility phase is smooth. This implies a rather large number of telescopes, possibly a few thousands for a star resolved in 200×200 elements. Workable trade-offs between these methods and those using image sharpness criteria on contrasted parts of the star, such as its edge, have to be explored.

## 5. Array concepts for planet imagery from the ground and from space

The ground-based OVLA concept can probably be extrapolated to 10 km size if suitable sites are found. The variants proposed for orbital or Moon-based operation can probably operate with 100 km sizes. Also, the number and size of the telescopes can reach the values mentioned above: 300 of 1.5 m, or 80 of 4 m, or 30 of 8 m. On Earth, with suitable phasing techniques, the 300 smaller telescopes can provide simultaneous snapshot images of the
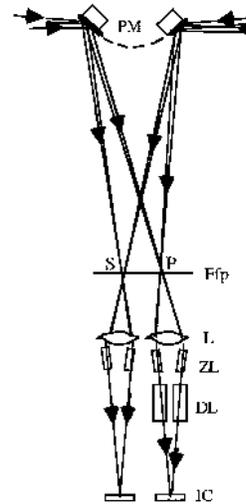


**Fig. 5.** Principle of beam recombiner for blind phasing in the planet image: the star (S) and planet (P) images in the recombined focal plane Ffp are separately re-imaged, in the Michelson mode, through lenses L and sets of zoom lenses ZL onto cameras IC. Piezo-ceramic mounts PM provide the common fast phasing needed to compensate atmospheric effects for both the star and planet. Slower delay lines DL provide the additional differential phasing, a priori known, needed to compensate the first-order departure from isoplanaticity of Michelson arrays, and the higher orders caused by aberrations in the optical train. Different zoom settings can be used for the star and planet images

star and its Jupiter-like planets, with full resolution. A few ground-based sites, at high altitudes, may allow the free-air propagation of coudé beams for 5 km with tolerable levels of atmospheric disturbance. Vacuum tunnels may also be considered but they preclude mobile telescopes, and therefore imply the use of optical delay lines.

Optical fibers can also be used, instead of conventional coudé trains, to collect light from the telescopes and bring it towards the recombined focus. The outputs of single-mode fibers can be bundled together, in such a way as to reproduce the aperture pattern, at some distance from the recording camera. If the optical path difference is adjusted, possibly by stretching the fibers, the interference pattern generated on the camera behaves like those considered above, according to Eq. (4), and images can similarly be obtained directly.

With 1.5 m afocal telescopes serving as array elements, a 1″ field requires a 400 mm collecting aperture at 5 km (half a 10 km baseline) if the afocal magnification is 10. In the OVLA concept, the balancing of the optical paths is achieved by moving the telescopes during the observation instead of using optical delay lines. On Earth, the maximal velocity required for the motion is 150 m/hour per kilometer of baseline. It can be decreased greatly by moving the central recombining optics itself along an East-West track.

8 m telescopes can be built with spherical mounts having an open frame steel structure, and hexapod translators are of interest for bi-directional mobility on the natural ground or an array of posts.

In space, high orbits appear compatible with the operation of free-flying telescopes forming a stabilized array with 10 to 100 km size. Following the TRIO proposal (Authier et al. 1985), involving small solar sails attached to each free-flyer for controlling its motion, the European Space Agency is now studying the use of ion thrusters. Lunar sites also appear usable, but provide severe constraints.

A major advantage of space, with its nearly perfect "seeing", is the much longer life-time of the speckles, including the dark speckles. Their fluctuation results from thermal deformations of the telescope components. It allows a more efficient use of speckle darkening algorithms, which can be applied in active forms, using active optical elements. Also, faint background stars located within arcseconds from the planet's own parent star may provide a more convenient reference for phasing.

## 6. Conclusion

The analysis of image formation in extended versions of Michelson's stellar interferometer shows that resolved images of extra-solar planets are theoretically feasible, both from the ground and from space. In practice, current projects for multi-telescope arrays of 600 m size will require upgrading to tackle such goals. As the technical difficulties will become mastered, a continuous evolution towards larger sizes is to be expected. Jupiter-like planets at 5 pc can be imaged from Earth with 10 km arrays, while Earth-like planets at 5 pc require 100 km arrays, preferably installed in space. Because such images can also yield spectra for each of their resolved elements, they should provide a better diagnostic for the presence of life, and possibly civilisation, than would spectra of unresolved-planets. Other objects such as pulsars, galactic nuclei and QSO's are also candidates for high resolution imaging.

## References

Angel J.R.P., 1994, Nat 368, 203-207

Authier B., Rabout P., Labeyrie A., 1985, in Kilometric Optical Arrays in Space, ESA SP-226. In: Longdon N., Melita O. (eds.) ESA, Paris, 79-84

Bonneau D., Josse M., Labeyrie A., 1975, in Image processing techniques in Astronomy. In: de Jager C., Nieuwenhuijzen H. (eds.). Dordrecht, Reidel, 403-409

Bracewell R.N., MacPhie R.H., 1979, Icarus 38, 136-147

Brown R.A., 1990, in Astrophysics from the Moon. In: Mumma M.J., Smith H.J. (eds.) AIP Conf. Proc. 207, New York, AIP, 87-94

Burke B.F., 1986, Nat 322, 340-341

KenKnight C.E., 1977, Icarus 30, 422-433

Labeyrie A., 1975, ApJ 196, L71-L75

Labeyrie A., Kibblewhite J., de Graauw T., Roussel H., Noordam J., Weigelt G., 1982, Very Long Baseline Interferometry Techniques, Toulouse, CEPAD, 477-488

Labeyrie A., Lemaître G., Koechlin L., 1986, SPIE 628, Advanced Technology Optical Telescopes III. In: Barr L.D. (ed.), Bellingham, SPIE, 323-332

Labeyrie A., Cazalé C., Gong S., et al., 1992, High Resolution Imaging by Interferometry II. In: Beckers J.M., Merkle F. (eds.). Garching, ESO, 765-773

Labeyrie A., 1995, A&A 298, 544-546

Malbet F., Shao M., Yu J.W., 1994, SPIE 2201, Adaptive Optics in Astronomy. In: Ealey M.A., Merkle F. (eds.), Bellingham, SPIE, 1135-1144

Mariotti J.M., 1992, Proc. ESA, Coll. on Targets for Space Based Interferometry, Beaulieu, France

Mayor M., Queloz D., 1995, Nat 378, 355-359

Mourard D., Tallon-Bosc I., Blazit A., et al., 1994, A&A 283, 705-713

Tallon M., Tallon-Bosc I., 1992, A&A 253, 641-645